Journal of Power Sources 222 (2013) 169–176

Contents lists available at SciVerse ScienceDirect

Journal of Power Sources

journal homepage: www.elsevier.com/locate/jpowsour

Dealloyed $PdCu_3$ thin film electrocatalysts for oxygen reduction reaction

Ruizhi Yang [a,b,c,*], Weiyong Bian [a], Peter Strasser [d], Michael F. Toney [b,c]

[a] School of Energy, Soochow University, Suzhou, Jiangsu 215006, China
[b] Stanford Institute for Materials and Energy Science, SLAC National Accelerator Laboratory, Menlo Park, CA 94025, USA
[c] Stanford Synchrotron Radiation Light Source, SLAC National Accelerator Laboratory, Menlo Park, CA 94025, USA
[d] The Electrochemical Energy, Catalysis, and Materials Science Laboratory, Department of Chemistry, Chemical Engineering Division, Technical University Berlin, 10623 Berlin, Germany

HIGHLIGHTS

- Dealloyed Pd–Cu thin films show higher ORR activity compared to pure Pd.
- Enhancement of ORR activity is attributed to the strain in the Pd surface layer.
- Dealloying and the ORR activity are dependent on the noble component of alloy.
- The relationship between the structure and ORR activity is better understood.

ARTICLE INFO

Article history:
Received 4 July 2012
Received in revised form
20 August 2012
Accepted 22 August 2012
Available online 1 September 2012

Keywords:
Dealloyed
Thin film
Electrocatalysts
Oxygen reduction reaction

ABSTRACT

The catalytic activity of electrochemically dealloyed $PdCu_3$ thin films for oxygen reduction reaction (ORR) in acidic media has been studied by using a rotating disk electrode (RDE). The dealloyed $PdCu_3$ thin films show a ~2.0 fold increase in the specific oxygen reduction activity over pure Pd thin films. The structure of electrochemically dealloyed $PdCu_3$ thin films has been investigated at an atomic scale by synchrotron-based anomalous X-ray diffraction (AXRD). AXRD reveals that a Pd enriched surface layer is formed in the dealloyed film and a compressive lattice strain exists in this Pd surface layer. The enhanced catalytic activity of dealloyed Pd–Cu films for the ORR is primarily due to the compressive strain in the surface layer. We compare the structure–composition–catalytic activity relationships in dealloyed Pd–Cu thin films to related results on dealloyed Pt–Cu thin films. These studies show that dealloying and the resulting structure and the ORR activity are dependent on the nature of the noble component of alloy.

1. Introduction

Polymer electrolyte membrane fuel cells (PEMFC) convert the hydrogen and oxygen directly into electricity and water and are considered to be a major source of clean energy [1]. It is well known that the efficiency of these fuel cells is limited by the slow kinetics of the oxygen reduction reaction (ORR) at the cathode [2,3]. Platinum and Pt-based alloy are widely used as the electrocatalysts for ORR. However, Pt is expensive and scarce, which hinders the widespread commercialization of PEMFCs. Research efforts have been focused on reducing the Pt content or replacing Pt with less expensive materials. More abundance and lower price of Pd makes it an alternative electrocatalyst for ORR. However, the intrinsic ORR activity of Pd is noticeably lower than that of Pt [4,5]. The combination of Pd with other metals, such as Ni [6,7], Fe [8,9], Sn [10], Co [11,12], Ti [13], Cr [14] and Cu [15–17], has been reported to show enhanced activity as well as stability compared to pure Pd. Therefore Pd-based alloys have attracted much attention and were introduced as ORR catalysts for PEMFC applications. The origin in the enhancement of ORR activity of PdM alloy has been attributed to the modification of the electronic structure of Pd upon alloying with the base metal [5,18,19].

The surface electronic structure and the electrocatalytic activity of PdM or PtM alloy can also be modified with Pd or Pt overlayers formed at the surface [20–24]. Dealloying is a process that a less noble component is selectively dissolved from a bimetallic alloy with the more noble component accumulating onto the surface. This process is an important pathway to create noble metal surface overlayers [25–30]. It has been shown that dealloyed Pt–Cu nanoparticle electrocatalysts formed by electrochemically dealloying Cu-rich precursors (i.e. $PtCu_3$) show uniquely high ORR

* Corresponding author. School of Energy, Soochow University, Suzhou, Jiangsu 215006, China. Tel.: +86 512 65221519.
E-mail addresses: yangrz@suda.edu.cn, rzyang999@hotmail.com (R. Yang).

0378-7753/$ – see front matter © 2012 Elsevier B.V. All rights reserved.
http://dx.doi.org/10.1016/j.jpowsour.2012.08.064

activities [31–35]. We have gained insights into the structure and the resulting mechanism of ORR enhancement of dealloyed Pt–Cu alloy in our previous studies on dealloyed $PtCu_3$ nanoparticles [34,35], on dealloyed $PtCu_3$ thin films [36] and on dealloyed $Cu_3Pt(111)$ single crystals [37]. Our results have shown that dealloyed Pt–Cu consists of a Pt enriched surface layer and Cu depleted interior and that the Pt surface layer is compressively strained. The compressive strain in the surface layer results in the downshift and broadening of the Pt d-band, which leads to a weaker oxygen bond strength and thus an ORR activity enhancement in the dealloyed Pt–Cu alloy.

The structure and ORR activities of the electrochemically dealloyed binary (like PtM_3 alloy, M = Cu, Co, Ni) and ternary (like $PtNi_3M$ alloy, M = Cu, Co, Fe, Cr) Pt-based alloy electrocatalysts were found to be dependent on the nature and initial composition of the non-noble component [35,38]. To understand the effect of noble component on dealloying and the resulting structure and ORR activity of binary electrocatalysts, we report here the structure and catalytic activities for ORR of dealloyed $PdCu_3$ thin films. We also compare the results on dealloyed $PdCu_3$ thin films to related results on dealloyed $PtCu_3$ thin films. In contrast to relatively non-uniform, multiphase structure, size polydispersity and shape diversity of nanoparticles, the structure of uniform, single phase and well-alloyed thin films can be accurately characterized, allowing the structure–composition–catalytic activity relationships to be better understood. Synchrotron-based anomalous X-ray diffraction (AXRD) is used to study the detailed structure of the dealloyed Pd–Cu thin films at an atomic scale. The Pd overlayer formed on the dealloyed Pd–Cu thin film is about 1.5 nm thick (6–7 monolayers), where the ligand effect (heterometallic bonding interactions between the surface atoms and the substrate atoms, active for one to three monolayers [39]) is very weak. The compressive strain in the surface layer accounts for the enhanced ORR activity of dealloyed Pd–Cu. The ORR activity enhancement factor (about 2.0 times that of Pd) in the dealloyed Pd–Cu thin films is smaller than that in similarly dealloyed Pt–Cu thin films (about 2.4 times that of Pt) reported in our previous study [36], despiting the fact that both of the films were prepared by the exactly same method using precursors with the same atomic ratio (i.e. 1:3 atomic ratio of Pd (Pt):Cu) and the thickness of both precursor films is the same. This activity difference is consistent with the observation that the compressive strain in the Pd surface layer of the dealloyed Pd–Cu thin films is smaller than that in the Pt overlayer of the dealloyed Pt–Cu thin films. This is caused by the larger thickness of Pd overlayers (~1.5 nm) formed in the dealloyed Pd–Cu films than that of Pt overlayers (~1.0 nm) formed in the dealloyed Pt–Cu films. The formation of thicker Pd overlayer in the surface is due to the fact that more Cu is dissolved from the Pd–Cu thin films compared to the Pt–Cu thin films as a result of faster diffusion of Pd than that of Pt in the surface during dealloying in the same solution.

2. Experimental

2.1. Sample preparation

The $PdCu_3$ thin films are prepared by the same process for preparing $PtCu_3$ thin films reported in our previous study [36]. The $PdCu_3$ as well as pure Pd thin films were prepared by a Metallica magnetron sputter system, reaching a base pressure of 1×10^{-7} Torr prior to deposition. The $PdCu_3$ and Pd sputtering targets (1.00 in. diameter, 0.125 in. thick and 99.99% pure, Atlantic Metals & Alloys, Inc. USA) were sputtered using a DC power supply under 5×10^{-3} Torr Ar (99.999%) and cleaned by sputtering for about 1 min to remove surface impurities prior to deposition. Films were deposited onto: 1) glassy carbon (GC) disks with a diameter of 5 mm (Pine Instruments) for electrochemical measurements, which were polished with 0.5 μm alumina suspension prior to use; and 2) 10 mm × 10 mm one-sided polished highly doped *n*-Si(100) wafers (P-doped, 4–6 Ωcm; UniversityWafer.com) for structural analysis and film thickness determination. Before deposition, the Si(100) substrates were successively degreased in acetone, ethanol and water for 15 min. Then the substrates were treated with fresh H_2SO_4/H_2O_2 solution (3:1, v/v) for 1 min to remove any trace of heavy metals and organic species. Finally the substrates were etched for 1 min in 5% HF to remove the oxide layer and thoroughly rinsed with ultrapure water. The electrical/ohmic contact, which was important for electrochemical treatments, was formed by sputtering a thin Au film on the back of the etched wafer. The thickness of both $PdCu_3$ and pure Pd films was 10 nm, which was determined using a Dektak 8 Advanced Development Profilometer (Veeco Instruments Inc.), and the estimated error is about 5%.

2.2. Synchrotron X-ray diffraction and anomalous X-ray diffraction

Synchrotron-based X-ray diffraction (XRD) of the as-deposited $PdCu_3$ and dealloyed Pd–Cu films on Si was performed on beam line 7-2 at Stanford Synchrotron Radiation Lightsource. The synchrotron radiation source provides a high incident X-ray intensity and allows variation of the X-ray energy which enables compositional sensitive analysis. The film samples were measured in a specular geometry with 1 milliradian analyzer collimation (Soller slit). The scattering intensity was recorded as a function of the scattering vector $Q = 4\pi\sin(2\theta/2)/\lambda$, where 2θ is the angle between the incident and diffracted X-rays and λ is the wavelength of the X-rays. The XRD data were first collected between Q of 2.0 and 6.5 $Å^{-1}$ at 8800 eV. For the anomalous X-ray diffraction (AXRD), profiles were measured in a shorter Q range (2.0–4.0 $Å^{-1}$) around the (111) peak at 22 energies between 8800 eV and 9160 eV, across the X-ray absorption edge of Cu at 8980 eV. The (111) peak in the XRD profile was fitted to either one or two peaks with Lorentzian function using Origin 8.0 (Origin Lab Corporation). The integrated area (A_{indiv}) of each individual fitted peak and the total integrated area (A_{total}) of (111) peak were obtained at each X-ray energy. A_{total} or A_{indiv} is directly proportional to the structure factor $|F|^2_{(111)}$ of the sample at that X-ray energy. The compositional information (molar fractions) of Pd and Cu, xPd and xCu = 1 − xPd, of the peaks are obtained by modeling $|F|^2_{(111),expt}$ using the relationship between the structure factor and the X-ray energy E [40]:

$$|F|^2_{(111)} = \left| x_{Pt}\left[f_{Pt,111}(Q) + f'_{Pt}(E) + i f''_{Pt}(E)\right] + x_{Cu}\left[f_{Cu,111}(Q) + f'_{Cu}(E) + i f''_{Cu}(E)\right]\right|^2 \quad (1)$$

Here $f(Q)$ is the atomic scattering factor, $f'(E)$ is the real part of the anomalous scattering factor and $f''(E)$ is the imaginary part of the anomalous scattering factor, which are all known and tabulated [41]. The corresponding unit cell parameters were deduced from the average fitted peak position obtained at each energy.

2.3. X-ray Photoelectron Spectroscopy (XPS) analysis of the surface composition

Surface analysis of the films on the GC disks was performed with an SSI (Surface Science Instruments) X-ray Photoelectron Spectroscopy (XPS) spectrometer equipped with a hemispherical analyzer and using a monochromatized Al Kα (1486 eV) source with a 250 × 1000 μm illumination spot. The measurement parameters were as follows: 20 eV pass energy, 0.1 eV energy increments. The measurements were all performed on the films on the GC disks. The

spectra were corrected for the background using the Shirley approach and the composition of the films was determined by measuring the ratio of Pd3d to Cu2p intensities (integrated peak area) normalized by their respective sensitivity factors [42]. The probing depth (about 1.9 nm) is obtained from the inelastic mean free path of Pd3d and Cu2p estimated from TPP-2M equation described by Tanuma et al. [43].

2.4. Electrochemical measurements

The electrochemical measurements were conducted in a standard three-electrode electrochemical cell at room temperature. A Pt-foil was used as the counter electrode, and a Ag/AgCl (3 M Cl^-, Cypress) reference electrode was used in a double-junction reference chamber. The potential of the Ag/AgCl reference electrode was calibrated versus the reversible hydrogen electrode (RHE). All potentials reported in this study refer to that of RHE. The electrolyte was 0.1 M $HClO_4$ solution prepared from double-distilled $HClO_4$ (70%, Sigma Aldrich) and ultrapure water (Millipore, 18.2 MΩ cm). The working electrodes were the thin film-deposited GC disks mounted in a disk-interchangeable rotating disk electrode (RDE, Pine Instruments) or the thin film-deposited Si wafers, which were mounted to a custom-made stainless steel shaft using a Teflon holder. The geometrical surface area of GC disk electrode and Si(100) electrode exposed to the electrolyte was 0.196 cm^2 and 0.503 cm^2, respectively. Measurements of the electrocatalytic activity of the different catalysts for oxygen reduction reaction (ORR) were all performed on the GC disk electrodes, while the $PdCu_3$ films on Si after dealloying were used for the structure analysis because of almost zero background X-ray scattering of Si(100) substrates.

The electrolyte was deaerated by purging high-purity Ar gas into the electrolyte for at least 30 min before each electrochemical measurement. The working electrode was immersed into the Ar-saturated electrolyte under potential control and held at 0.05 V (RHE) until the measurements commenced. The dealloying was performed by 400 cyclic voltammetry (CV) potential scans between 0.05 V and 1.0 V at a scan rate of 500 mV s^{-1} in Ar-saturated 0.1 M $HClO_4$ solution, which is similar to the procedure described in our previous study [36]. After steady state CVs were obtained, one CV with a scan rate of 50 mV s^{-1} was collected on the dealloyed Pd–Cu on GC disk. The electrochemical surface area (ECSA) of Pd-alloy samples could not be obtained from the hydrogen desorption region due to the dissolution of hydrogen into the bulk of Pd. The ECSA of the samples was determined from the charge involved in the reduction of the surface oxide layer, from the cyclic voltammograms in 1.0 M H_2SO_4 solutions, assuming a value of 405 μC cm^{-2} for a monolayer coverage [44,45]. The roughness factor (RF) was obtained from the ratio of ECSA to the geometric surface area (0.196 cm^2)

$$\mathrm{RF} = \mathrm{ECSA}/\mathrm{SA}_{\mathrm{geo}} \tag{2}$$

The ORR electrocatalytic activity of the dealloyed Pd–Cu and pure Pd films on the GC disks was studied with RDE using a rotator (AFMSRX, Pine Instruments). The electrolyte was purged with high-purity O_2 gas for at least 30 min to ensure O_2 saturation. Linear sweep voltammetry (LSV) measurements during oxygen reduction were performed in O_2-saturated 0.1 M $HClO_4$ by sweeping the potential from 0.05 V anodically to 1.0 V [3,31,36] at 20 mV s^{-1} with the electrode rotated at 400, 900, 1600 and 2500 rpm and O_2 gas purged into the solution at a rate of 1 L min^{-1} through a 2 μm fritted tube (Ace Glass). The faradaic current density, i.e., the current due to the oxygen reduction alone, was obtained by subtracting the capacitive current (the current measured from the CV under Ar) from the ORR data and then normalized by the geometric surface area,

$$j = -\left(j_{\mathrm{ORR}} - j_{\mathrm{capacitive,Ar-CV}}\right)\Big/\mathrm{SA}_{\mathrm{geo}} \tag{3}$$

The kinetic current density for the ORR was derived from the Koutecky–Levich equation:

$$1/j = 1/j_{\mathrm{k}} + 1/j_{\mathrm{d}} = 1/j_{\mathrm{k}} + 1\Big/\left(B\omega^{1/2}\right) \tag{4}$$

where j is the measured disk current density; j_{k} and j_{d} are the kinetic and diffusion limiting current densities, respectively; B is the so-called "B-factor", which is given by the following equation:

$$B = 0.62nFD_{\mathrm{O_2}}\upsilon^{-1/6}C_{\mathrm{O_2}}, \tag{5}$$

where $D_{\mathrm{O_2}}$ is the diffusion coefficient of O_2 ($D_{\mathrm{O_2}} = 1.93 \times 10^{-5}$ cm^2 s^{-1}), υ is the kinetic viscosity of the solution ($\upsilon = 1.009 \times 10^{-2}$ cm^2 s^{-1}), $C_{\mathrm{O_2}}$ is the concentration of O_2 dissolved in electrolyte ($C_{\mathrm{O_2}} = 1.26 \times 10^{-3}$ mol L^{-1}) [46,47], F is the Faraday constant, and n is the apparent number of electrons transferred in the reaction. ω is the electrode rotation speed. The kinetic current density (normalized by the geometric surface area) was divided by the RF factor to obtain the ECSA normalized kinetic current density

$$j_{\mathrm{s,Pt}} = j_{\mathrm{k}}/\mathrm{RF} \tag{6}$$

The ohmic resistances in the electrode contacts and electrolyte solution were assumed to be the same for dealloyed Pd–Cu and pure Pd and were not included in the corrections. The specific activity was established from the ECSA normalized kinetic current density measured at 0.88 V vs. RHE.

3. Results and discussion

3.1. Structure of dealloyed Pd–Cu thin films

Fig. 1 shows the X-ray diffraction profiles of the as-deposited $PdCu_3$, dealloyed Pd–Cu and as-deposited Pd films on Si(100). Both the as-deposited $PdCu_3$ and Pd films show single phase face centered cubic (FCC) structures. The average lattice constants obtained from the best fitting for the as-deposited $PdCu_3$ and Pd film

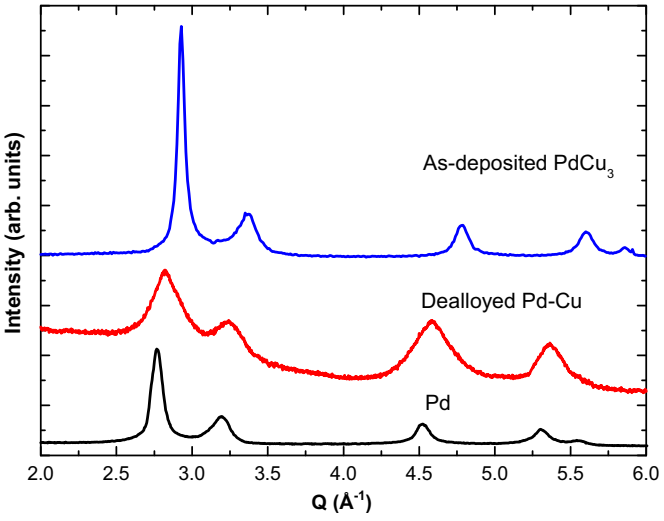

Fig. 1. X-ray diffraction profiles of as-deposited $PdCu_3$, dealloyed Pd–Cu and as-deposited Pd thin film samples on Si(100).

are 3.708 and 3.891 Å, respectively, which are in close agreement with those reported for bulk materials [48]. For the dealloyed Pd–Cu film, it is clearly observed that the diffraction peaks shift toward lower Q and are broader compared to the as-deposited $PdCu_3$, indicating that Cu is leached from $PdCu_3$ alloy and that the structure becomes disordered with a smaller grain size. The asymmetric feature of the diffraction peaks suggests that a non-uniform structure is formed in the film after dealloying.

To obtain the detailed structure of the dealloyed Pd–Cu thin film and insight into the dealloying, anomalous X-ray diffraction (AXRD) was performed in the energy range of the Cu absorption K edge (8980 eV). In AXRD, peak positions yield average lattice parameters for the films, and the relationship between scattering intensity and energy provides the chemical composition of the scattering alloy phase. AXRD profiles of the dealloyed Pd–Cu at several energies are shown in Fig. 2a. As the X-ray energy approaches the Cu edge, a decrease in scattering intensities of the (111) and (200) Bragg reflections is observed. This intensity decrease is related to the drop in scattering power of Cu near the Cu absorption edge and allows the Cu content of the scattering phase to be accurately determined. Fig. 2b shows the fitting of a typical profile of the dealloyed Pd–Cu film. The (111) reflection of the dealloyed Pd–Cu film is asymmetric and is fitted to two peaks (peak 1 and peak 2). As the Cu edge energy is approached, the integrated intensity for peak 2 (Fig.2d) of the dealloyed Pd–Cu drops while the integrated intensity for peak 1 does not decrease. This shows that the phase causing peak 1 is free of Cu to within our measurement ability of about 4%. The surface composition is determined to be nearly pure Pd ($Pd_{94}Cu_6$) form the XPS data. Therefore peak 1 corresponds to a nearly pure Pd surface layer and peak 2 corresponds to the interior region of dealloyed Pd–Cu still containing Cu. The dealloyed Pd–Cu consists of a Pd enriched surface layer and Cu depleted alloy interior.

The (111) diffraction peak for the Pd surface layer (peak 1) is centered at $Q = 2.808 \pm 0.007$ Å^{-1} (average position from AXRD). The error was determined from the average (111) peak positions at 22 energies between 8800 eV and 9160 eV obtained from the AXRD. This error corresponds to about 96% confidence interval since the measurement ability of AXRD is within 4%. The corresponding lattice constant ($a_{surface}$) is 3.875 ± 0.007 Å, which is smaller than that of pure Pd (a_{Pd} = 3.891 Å). The surface region thus has a compressive strain ($S = (a_{surface} - a_{Pd}/a_{Pd}) \times 100$) of $-0.41 \pm 0.10\%$ with respect to pure Pd. The average chemical compositions of the dealloyed Pd–Cu films (overall, i.e. peak 1 + peak 2) and the interior region of the dealloyed Pd–Cu films (peak 2) are determined from the relationship between the integrated intensity and X-ray energy based on equation (1). The fits from equation (1) for the (111) integrated intensity of the dealloyed Pd–Cu (overall, i.e. peak 1 + peak 2) and of the interior region of the dealloyed Pd–Cu films (peak 2) as a function of energy are shown in Fig.2c and d, respectively. Details on the composition and lattice parameters of dealloyed Pd–Cu film are summarized in Table 1, the corresponding results of dealloyed Pt–Cu films are also included for comparison.

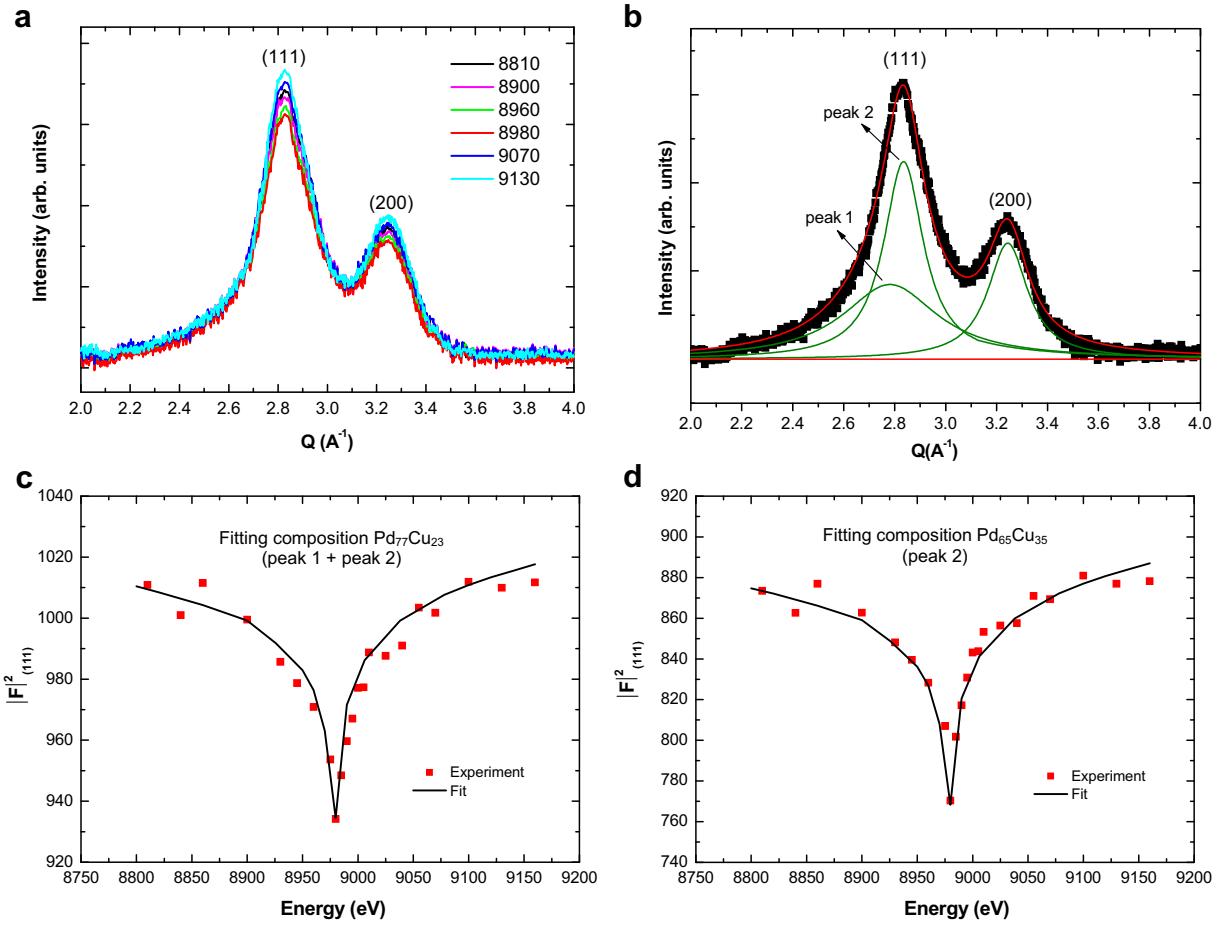

Fig. 2. (a) Anomalous X-ray diffraction (AXRD) profiles of the dealloyed Pd–Cu film as a function of the scattering vector Q at indicated energies. (b) Fitting (Lorentz function) of a typical XRD profile of the dealloyed Pd–Cu thin film taken at 8810 eV. The fitting from the calculation (equation (1)) for the integrated intensity of (111) reflection of the dealloyed Pt–Cu thin film (c) and interior of dealloyed Pt–Cu thin film (d) as a function of X-ray energy.

Table 1
Composition and the lattice parameters for the as-deposited $PdCu_3$, dealloyed Pd–Cu, as-deposited $PtCu_3$ and dealloyed Pt–Cu thin films.

Sample	Bulk composition (AXRD)	Surface composition (XPS)	Lattice parameter (Å)
As-deposited $PdCu_3$	$Pd_{25}Cu_{75}$	$Pd_{25}Cu_{75}$	3.708
Dealloyed Pd–Cu (overall)	$Pd_{77}Cu_{23}$	$Pd_{94}Cu_6$	–
Dealloyed Pd–Cu (interior)	$Pd_{65}Cu_{35}$	–	3.794
Dealloyed Pd–Cu (surface layer)	Pd	–	3.875
As-deposited $PtCu_3$	$Pt_{26}Cu_{74}$	$Pt_{25}Cu_{75}$	3.716
Dealloyed Pt–Cu (overall)	$Pt_{68}Cu_{32}$	$Pt_{91}Cu_9$	–
Dealloyed Pt–Cu (interior)	$Pt_{59}Cu_{41}$	–	3.802
Dealloyed Pt–Cu (surface layer)	Pt	–	3.897

The surface composition and bulk composition measured from XPS and AXRD for the as-deposited films are all $Pd_{25}Cu_{75}$ (see Table 1), showing that the as-deposited $PdCu_3$ film is uniformly alloyed. After dealloying, the resulting Pd–Cu film becomes inhomogeneous as evidenced from the difference between the surface composition ($Pd_{94}Cu_6$), the interior composition ($Pd_{65}Cu_{35}$) and the overall composition ($Pd_{77}Cu_{23}$) of dealloyed Pd–Cu film. It's important to note that Cu content either in the overall or interior region of dealloyed Pd–Cu ($Pd_{77}Cu_{23}$ for overall and $Pd_{65}Cu_{35}$ for interior) is smaller than that in the corresponding region of dealloyed Pt–Cu ($Pt_{68}Cu_{32}$ for overall and $Pt_{59}Cu_{41}$ for interior) although the atomic ratio of constituent elements (1:3 atomic ratio of Pd:Cu or Pt:Cu) and thickness (10 nm) of both precursor films are the same. This shows that more Cu is dissolved from $PdCu_3$ films as compared with $PtCu_3$ films after dealloying in the same solution.

The as-deposited $PdCu_3$ thin film is uniform, well alloyed and single phase as shown by the XRD profiles (Fig.1). After dealloying, most Cu is removed from the surface and partially from the interior, leaving a nearly pure Pd enriched surface layer with compressive strain of 0.41 ± 0.10% (relative to Pd) which covers a Cu depleted interior. This is similar to the structure of dealloyed Pt–Cu from $PtCu_3$ thin film precursor reported in our previous work [36]. It is worth mentioning that the lattice parameter of the interior region of the dealloyed Pd–Cu (peak 2) estimated using Vegard's rule ($a = 3.891x + 3.615(1 - x)$) for Pd_xCu_{1-x}, the interior composition ($Pd_{65}Cu_{35}$) is 3.794 Å, which is in excellent agreement with the lattice parameter of 3.796 Å obtained from the peak position (peak 2) by AXRD. From the AXRD derived surface and interior compositions and lattice parameters, the thickness of the Pd surface layer in the dealloyed Pd–Cu can be estimated from the following equation (see the details for equation derivation in our previous study [36]), assuming the atomic composition for the as-deposited film, dealloyed film and interior region of dealloyed film is Pt_xCu_{1-x} ($0 < x < 1$), Pt_yCu_{1-y} ($0 < y < 1$) and Pt_zCu_{1-z} ($0 < z < 1$), respectively. The thickness of the Pd surface layer of dealloyed film calculated from the equation is about 1.5 nm (6–7 Pd monolayers).

3.2. Catalytic activity of dealloyed Pd–Cu thin films for oxygen reduction

Cyclic voltammetry (CV) of a typical dealloyed Pd–Cu thin film on GC disks in 0.1 M $HClO_4$ after subtracting the double layer charge are shown in Fig. 3, which is compared with pure Pd film prepared with the same method. The CV of dealloyed Pd–Cu resembles that of pure Pd. A well-defined voltammetric profile of hydrogen absorption/desorption and hydrogen evolution can be seen in the potential region of 0–0.3 V. In the potential region of 0.6–0.8 V, it is noticed that the onset potential for the Pd oxide formation in the positive-going sweep as well as that for the oxide reduction in the negative-going sweep is shifted to more positive potential for dealloyed Pd–Cu as compared to pure Pd. This suggests that the Pd oxide formation/adsorption of oxygenated species are inhibited on dealloyed Pd–Cu [31,49,50], which is beneficial to the oxygen adsorption at low potential and thus the ORR kinetic enhancement [49,50]. The ECSAs of dealloyed Pd–Cu and pure Pd were determined from the charge for the reduction of the surface Pd oxide layer, from the cyclic voltammograms in 1.0 M H_2SO_4 solutions. The ECSA of dealloyed Pd–Cu (0.745 cm^2) is about 2.1 times that of pure Pd (0.355 cm^2). The roughness factors (ratio of ECSA to geometric surface area) for dealloyed Pd–Cu and pure Pd are 3.8 and 1.8, respectively, showing a rougher surface is formed on dealloyed Pd–Cu films due to leaching of Cu.

The polarization curves for the ORR on the dealloyed Pd–Cu thin film at different rotation rates are shown in Fig. 4a. They all reached well-defined diffusion limiting currents. Fig. 4b shows the corresponding Koutecky–Levich plots obtained from the inverse current density (j^{-1}) as a function of the inverse of the square root of the rotation rate ($\omega^{-1/2}$) for dealloyed Pd–Cu at 0.65, 0.75, 0.80 and 0.83 V, respectively. These plots are linear and parallel, indicating the first-order dependence of the kinetics of ORR on the dealloyed Pd–Cu surface. Each straight line intercept corresponds to the kinetic current i_k. The "B-factor" for dealloyed Pd–Cu is 0.148 mA cm^{-2} $\omega^{-1/2}$, determined from the slope of Koutecky–Levich plots, which is in good agreement with the theoretical value of 0.151 mA cm^{-2} $\omega^{-1/2}$ calculated for a four-electron-reduction process from the equation (5). Hence the ORR reactions on the surface of dealloyed Pd–Cu thin film proceed with $n = 4$ e^- reaction pathway.

The comparison between ORR activities on dealloyed Pd–Cu, pure Pd, dealloyed Pt–Cu and pure Pt films is shown in Fig. 5a. The currents shown were measured at 1600 rpm and normalized by the geometric surface area. The ORR activity increases as follows: Pd < dealloyed Pd–Cu < Pt < dealloyed Pt–Cu. There is a positive shift of 50 mV in the half-wave potential of dealloyed Pd–Cu as compared to pure Pd, which is higher than the positive shift of 36 mV in the half-wave potential of dealloyed Pt–Cu as compared to pure Pt. This clearly shows that dealloyed Pd–Cu is more active than pure Pd and is very close to the activity of pure Pt. The

$$\frac{t_{surface}}{t_{as-deposited}} = \frac{t_{dealloyed}}{t_{as-deposited}} \times \frac{1}{\left(1 + \frac{t_{interior}}{t_{surface}}\right)} = \frac{a^3_{surface}x\left(y-z\right) + a^3_{interior}x\left(1-y\right)}{a^3_{as-deposited}y\left(1-z\right)} \times \frac{1}{\left(1 + \frac{a^3_{interior}\left(1-y\right)}{a^3_{surface}\left(y-z\right)}\right)}$$
$$= \frac{\left[a^3_{surface}x\left(y-z\right) + a^3_{interior}x\left(1-y\right)\right] \times a^3_{surface}\left(y-z\right)}{a^3_{as-deposited}y\left(1-z\right) \times \left[a^3_{surface}\left(y-z\right) + a^3_{interior}\left(1-y\right)\right]} \quad (7)$$

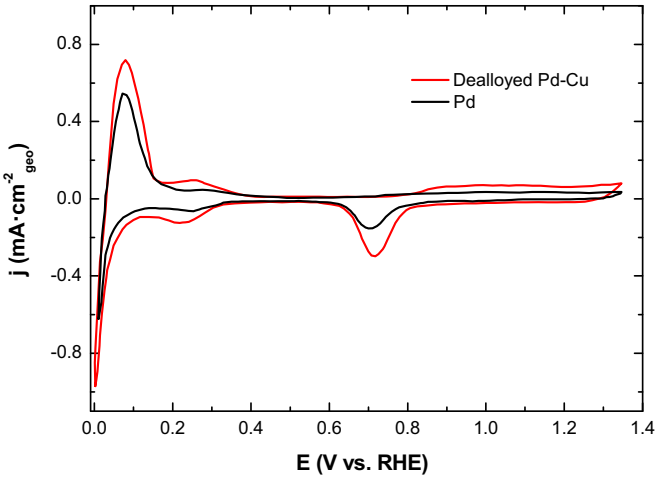

Fig. 3. Cyclic voltammetry of dealloyed Pd–Cu and pure Pd thin films. Experiments were conducted in Ar-saturated 0.1 M $HClO_4$ at 298 K with a sweep rate of 50 mV s^{-1}.

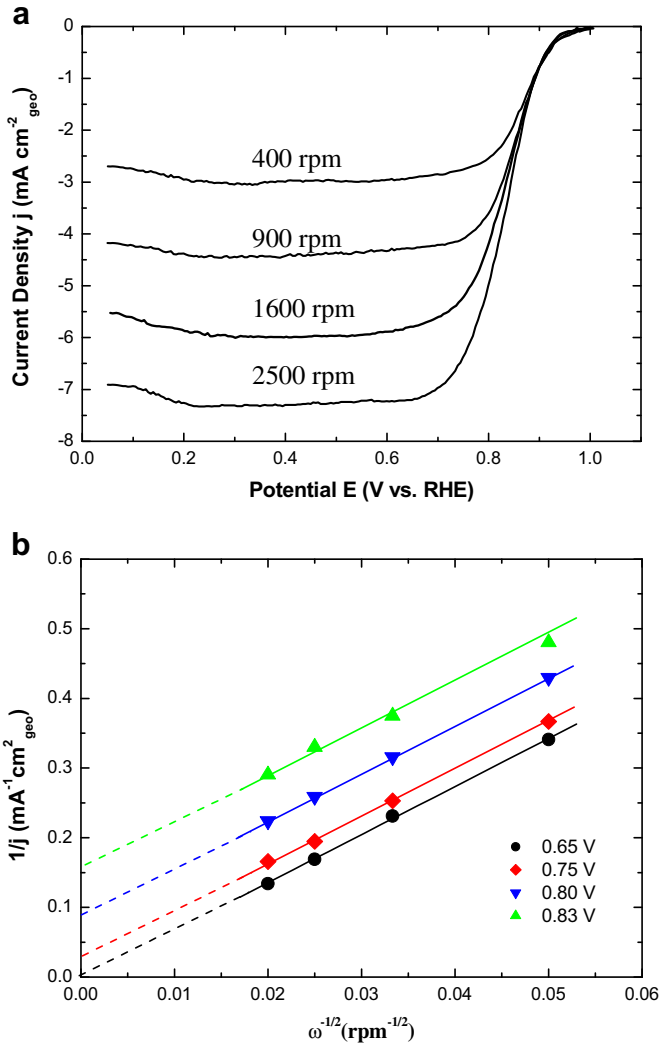

Fig. 4. (a) Polarization curves for the ORR on dealloyed Pd–Cu thin film at different rotation speeds. (b) Koutecky–Levich plots of dealloyed Pd–Cu thin film at various potentials. Experiments were conducted in O_2-saturated 0.1 M $HClO_4$ at 298 K with a sweep rate of 20 mV s^{-1}.

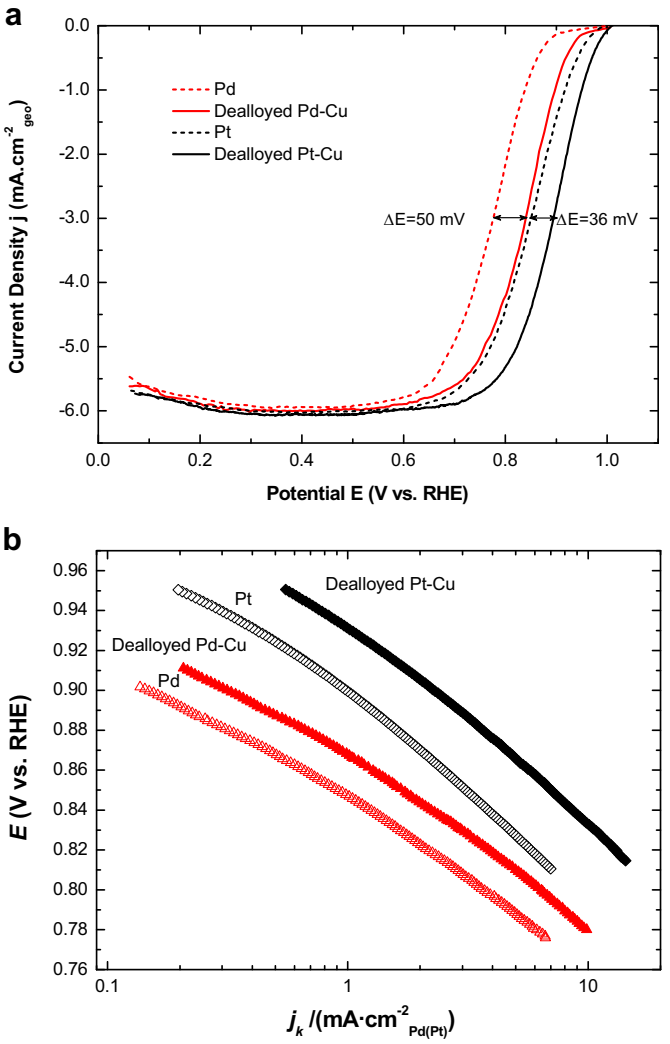

Fig. 5. (a) Oxygen reduction currents measured on dealloyed Pd–Cu and pure Pd thin films at a rotation speed of 1600 rpm. Arrows indicate the shift of half-wave potentials. (b) Pd surface normalized ORR activities of dealloyed Pd–Cu and pure Pd in (a). The ORR activities on dealloyed Pt–Cu and pure Pt thin films are also included for comparison. Experiments were conducted in O_2-saturated 0.1 M $HClO_4$ at 298 K with a sweep rate of 20 mV s^{-1}.

diffusion-current-corrected Tafel plots of specific ORR activity of these samples are shown in Fig. 5b. At 0.88 V, the specific activity of dealloyed Pd–Cu is 0.64 mA cm^{-2}_{Pd}, which is about 2.0 times that of Pd (0.31 mA cm^{-2}_{Pd}). The specific activity of dealloyed Pt–Cu is 3.67 mA cm^{-2}_{Pt}, which is about 2.4 times that of Pt (1.54 mA cm^{-2}_{Pt}). The structure and ORR activities of dealloyed Pd–Cu and dealloyed Pt–Cu thin films are summarized in Table 2. It is noticed that the specific activity enhancement for ORR on dealloyed Pd–Cu relative to pure Pd is lower than that on dealloyed Pt–Cu relative to pure Pt (Fig.5b, Table 2) although the half-wave potential shift of dealloyed Pd–Cu relative to pure Pd is higher than that of dealloyed Pt–Cu relative to pure Pt as shown in Fig.5a. This is because of the fact that the surface of dealloyed Pd–Cu is rougher than that of dealloyed Pt–Cu.

DFT studies of Shao [5] and Suo et al. [19] showed that the electronic structure of the Pd surface layer is modified by strain and the electron distribution between the Pd surface layer and its substrates (ligand effect), which in turn modifies the reactivity of the surface [5,19]. The Pd surface layer in our dealloyed Pd–Cu film consists of 6–7 Pd monolayers, where the ligand effect (active for one to three monolayers [39]) is very weak. Thus, the ORR activity

Table 2
The structure and ORR activities of dealloyed Pd–Cu and dealloyed Pt–Cu thin films.[a]

Sample	Thickness of Pd(Pt) overlayer (nm)	Strain (%)	Roughness factor (RF, cm^2 Pd $_{(Pt)}$ cm^{-2}_{geo})	Ratio of the specific activity of dealloyed Pd(Pt)–Cu relative to pure Pd(Pt) ($j_{s,Pd(Pt)-Cu}/j_{s,Pd(Pt)}$, 0.88 V)
Dealloyed Pd–Cu	1.5	−0.41	3.8	2.0
Dealloyed Pt–Cu	1.0	−0.66	2.7	2.4

[a] ORR activities were obtained in O_2-saturated 0.1 M $HClO_4$ at 1600 rpm at a scan rate of 20 mV s^{-1} at room temperature.

enhancement in the dealloyed Pd–Cu thin film is primarily attributed to the compressive strain in the Pd surface layer. The compressive strain reduces the adsorption energy of adsorbates by lowering the d-band center of the Pd surface layer and thus increases the activity for ORR [5,19,51] of dealloyed Pd–Cu relative to pure Pd. This is consistent with the CV results, where the peak potential of Pd oxide formation/adsorption of oxygenated species is positively shifted on dealloyed Pd–Cu relative to pure Pd (Fig. 3), suggesting a delayed oxide formation/adsorption of oxygenated species.

By combining the results on electrochemically dealloyed Pd–Cu thin films with our previous results on similarly dealloyed Pt–Cu thin films, we find that the dealloying and the resulting structure and catalytic activity of binary alloy electrocatalysts are dependent on the nature of the noble component. The thickness of Pd overlayer formed on the dealloyed Pd–Cu thin film (about 1.5 nm) is larger than that of Pt overlayer formed on the dealloyed Pt–Cu thin film (about 1.0 nm). This thicker layer relaxes more and thus the compressive strain in the Pd surface layer is smaller than that in the Pt surface layer, which results in the lower ORR activity enhancement of dealloyed Pd–Cu (about 2.0 times Pd) compared to that of dealloyed Pt–Cu thin films (about 2.4 times Pt). It has been reported that the surface mass transfer diffusion coefficients of Pd (1.1×10^{-20}) is two orders of magnitude larger than that of Pt (3.6×10^{-22}) in vacuum [52–54]. Moreover, there is strong experimental evidence that the surface diffusion along alloy/electrolyte interfaces is much faster than that in vacuum [55–57], likely related to the highly electrically polarized material/electrolyte interface [57]. The formation of thicker Pd surface layer in the dealloyed thin films is due to the fact that more Cu is dissolved from the surface layers, which results from faster diffusion of Pd than Pt in the surface during dealloying for the same solution [58,59].

4. Conclusions

Dealloyed Pd–Cu thin film electrocatalysts have shown high activities for ORR, which is about 2 times that of pure Pd. The compressive strain in the Pd overlayer resulting from electrochemical dealloying accounts for the ORR activity enhancement in the dealloyed Pd–Cu films. We find that dealloying and the resulting structure and hence the ORR activity are dependent on the nature of the noble component of the alloy. The compressive strain in the Pd surface layer of the dealloyed Pd–Cu films is smaller than that in the Pt surface layer of similarly dealloyed Pt–Cu films, so does the ORR activity, which likely results from the thicker Pd surface layer on the films due to faster diffusion of Pd than that of Pt during dealloying in the same solution. These findings provide a better understanding of the relationship between the structure, composition and ORR activities of dealloyed bimetallic electrocatalysts and also are helpful for the development of Pd-based electrocatalysts in PEMFCs.

Acknowledgments

Part of this work is supported by the Department of Energy, Office of Basic Energy Sciences, under contract DE-AC02-76SF00515 and under the auspices of the grant LAB04-20. R. Yang acknowledges support from the Young Researcher Science Foundation (SDY2011A04) managed by Soochow University, China. Portions of this research were carried out at the Stanford Synchrotron Radiation Light Source, a national user facility operated by Stanford University on behalf of the U.S Department of Energy, Office of Basic Energy Sciences.

References

[1] M.S. Dresselhaus, I.L. Thomas, Nature 414 (2001) 332.
[2] R.R. Adzic, in: J. Lipkowski, P.N. Ross (Eds.), Electrocatalysis, Wiley, New York, 1998, p. 197.
[3] H.A. Gasteiger, S.S. Kocha, B. Sompalli, F.T. Wagner, Appl. Catal. B 56 (2005) 9.
[4] E. Antolini, Energy Environ. Sci. 2 (2009) 915.
[5] M.H. Shao, P. Liu, J.L. Zhang, R. Adzic, J. Phys. Chem. B 111 (2007) 6772.
[6] G. Ramos-Sánchez, H. Yee-Madeira, O. Solorza-Feria, Int. J. Hydrogen Energy 33 (2008) 3596.
[7] J. Zhao, A. Sarkar, A. Mantiram, Electrochim. Acta 55 (2010) 1756.
[8] M. H.Shao, K. Sasaki, R.R. Adzic, J. Am. Chem. Soc. 128 (2006) 3526.
[9] M.R. Tarasevich, G.V. Zhutaeva, V.A. Bogdanovskaya, M.V. Radina, M.R. Ehrenburg, A.E. Chalykh, Electrochim. Acta 52 (2007) 5108.
[10] Md. R. Miah, M.T. Alam, T. Okajima, T. Ohsaka, J. Electrochem. Soc. 156 (2009) B1142.
[11] Y.-C. Wei, C.-W. Liu, Y.-W. Chang, C.-M. Lai, P.-Y. Lim, L.-D. Tsai, K.-W. Wang, Int. J. Hydrogen Energy 35 (2010) 1864.
[12] S. Tominaka, T. Hayashi, Y. Nakamura, T. Osaka, J. Mater. Chem. 20 (2010) 7175.
[13] J.L. Fernández, V. Raghuveer, A. Manthiram, A.J. Bard, J. Am. Chem. Soc. 127 (2005) 13100.
[14] K. Lee, O. Savadogo, A. Ishihara, S. Mitsushima, N. Kamiya, K. Ota, J. Electrochem. Soc. 153 (2006) A20.
[15] X. Wang, N. Kariuki, J.T. Vaughey, J. Goodpaster, J. Kumar, D.J. Myers, J. Electrochem. Soc. 155 (2008) B602.
[16] C. Xu, Y. Zhang, L. Wang, L. Xu, X. Bian, H. Ma, Y. Ding, Chem. Mater. 21 (2009) 3110.
[17] F. Fouda-Onana, S. Bah, O. Savadogo, J. Electroanal. Chem. 636 (2009) 1.
[18] M.H. Shao, J. Power Sources 196 (2011) 2433.
[19] Y. Suo, L. Zhuang, J. Lu, Angew. Chem. Int. Ed. 46 (2007) 2862.
[20] M.H. Shao, T. Huang, P. Liu, J. Zhang, K. Sasaki, M.B. Vukmirovic, R.R. Adzic, Langmuir 22 (2006) 10409.
[21] M. Arenz, T.J. Schmidt, K. Wandelt, P.N. Ross, N.M. Markovic, J. Phys. Chem. B 107 (2003) 9813.
[22] J.L. Zhang, M.B. Vukmirovic, Y. Xu, M. Mavrikakis, R.R. Adzic, Angew. Chem. Int. Ed. 44 (2005) 2132.
[23] J.R. Kitchin, J.K. Nørskov, M.A. Barteau, J.G. Chen, J. Chem. Phys. 120 (2004) 10240.
[24] R.R. Adzic, J. Zhang, S.K. Asaki, M.B. Vukmirovic, M.H. Shao, J.X. Wang, A.U. Nilekar, M. Mavrikakis, J.A. Valerio, F. Uribe, Top. Catal. 46 (2007) 249.
[25] T. Toda, H. Igarashi, H. Uchida, M. Watanabe, J. Electrochem. Soc. 146 (1999) 3750.
[26] M.T. Paffet, G.J. Beery, S. Gottesfeld, J. Electrochem. Soc. 135 (1988) 1431.
[27] M. Watanabe, K. Tsurumi, T. Mizukami, T. Nakamura, P. Stonehart, J. Electrochem. Soc. 141 (1994) 2659.
[28] S. Chen, W. Sheng, N. Yabuuchi, P.J. Ferreira, L.F. Allard, Y. Shao-Horn, J. Phys. Chem. C 113 (2009) 1109.
[29] Y. Ding, M. Chen, J. Erlebacher, J. Am. Chem. Soc. 126 (2004) 6876.
[30] H. Liu, P. He, Z. Li, J. Li, Nanotechnology (2006) 17.
[31] S. Koh, P. Strasser, J. Am. Chem. Soc. 129 (2007) 12624.
[32] P. Mani, S. Srivastava, P. Strasser, J. Phys. Chem. C 112 (2008) 2770.
[33] P. Strasser, S. Koh, J. Greeley, Phys. Chem. Chem. Phys. 10 (2008) 3670.
[34] C. Yu, S. Koh, J. Leisch, M.T. Toney, P. Strasser, Faraday Discuss. 140 (2008) 283.
[35] P. Strasser, S. Koh, T. Anniyev, J. Greeley, K. More, C. Yu, Z. Liu, S. Kaya, H. Ogasawara, M.F. Toney, A. Nilsson, Nat. Chem. 2 (2010) 454.
[36] R. Yang, J. Leisch, P. Strasser, M.F. Toney, Chem. Mater. 22 (2010) 4712.
[37] R. Yang, P. Strasser, M.F. Toney, J. Phys. Chem. C 115 (2011) 9074.
[38] P. Mania, R. Srivastava, P. Strasser, J. Power Sources 196 (2011) 666.
[39] A. Schlapka, M. Lischka, A. Gross, U. Kasberger, P. Jakob, Phys. Rev. Lett. 91 (2003) 016101.
[40] M. DeGraef, M.E. McHenry, Structure of Materials: an Introduction to Crystallography, Diffraction, and Symmetry, Cambridge University Press, Cambridge, 2007.

[41] V. Pecharsky, P.Y. Zavalij, Fundamentals of Powder Diffraction and Structural Characterization of Materials, Springer, New York, 2003.
[42] D. Briggs, M.P. Seah, Practical Surface Analysis, Wiley Interscience, New York, 1990.
[43] S. Tanuma, C.J. Powell, D.R. Penn, Surf. Interface Anal. 21 (1993) 165.
[44] T. Chierchie, C. Mayer, W.J. Lorenz, J. Electroanal. Chem. 135 (1982) 211.
[45] R. Pattabiraman, Appl. Catal. A Gen. 153 (1997) 9.
[46] N.M. Markovic, H.A. Gasteiger, P.N. Ross, J. Phys. Chem. 99 (1995) 3411.
[47] D.R. Lide, CRC Handbook of Chemistry and Physics, CRC Press, Boca Raton, FL, 1995.
[48] P. Villars, L.D. Calvert, Pearson's Handbook of Crystallographic Data for Intermetallic Phases, ASM International, Materials Park: OH, 1991.
[49] S. Mukerjee, S. Srinivasan, M.P. Soriaga, J. McBreen, J. Electrochem. Soc. 142 (1995) 1409.
[50] V.S. Murthi, R.C. Urian, S. Mukerjee, J. Phys. Chem. B 108 (2004) 11011.
[51] J.K. Norskov, J. Rossmeisl, A. Logadottir, L. Lindqvist, J.R. Kitchin, T. Bligaard, H. Jonsson, J. Phys. Chem. B 108 (2004) 17886.
[52] E.G. Seebauer, C.E. Allen, Prog. Surf. Sci. 49 (1995) 265.
[53] I. Beszeda, E.G. Gontier-Moya, D.L. Beke, Surf. Sci. 547 (2003) 229.
[54] Z.H. Zhang, Y. Wang, Z. Qi, W.H. Zhang, J.Y. Qin, J. Frenzel, J. Phys. Chem. C 113 (2009) 12629.
[55] J.M. Dona, J. Gonzalez Velasco, J. Phys. Chem. 97 (1993) 4714.
[56] J.J. Martinez Jubrias, M. Hidalgo, M.L. Marcos, J. Gonzalez Velasco, Surf. Sci. 266 (1996) 239.
[57] J. Erlebacher, J. Electrochem. Soc. 151 (2004) C614.
[58] J. Erlebacher, M.J. Aziz, A. Karma, N. Dimitrov, K. Sieradzki, Nature 410 (2001) 450.
[59] J. Erlebacher, R. Seshadri, MRS Bull. 34 (2009) 561.